Available online at www.sciencedirect.com
ScienceDirect
Journal of Molecular Graphics and Modelling 25 (2006) 345–352
Journal of Molecular Graphics and Modelling
www.elsevier.com/locate/JMGM

Characterization of the farnesyl pyrophosphate synthase of *Trypanosoma cruzi* by homology modeling and molecular dynamics

Lucas Sigman, Verónica Muriel Sánchez, Adrián Gustavo Turjanski *

Departamento de Química Inorgánica, Analítica y Química Física/INQUIMAE, Facultad de Ciencias Exactas y Naturales, Universidad de Buenos Aires/CONICET, Ciudad Universitaria, Pab. II, P. 3, C1428EHA Buenos Aires, Argentina

Received 15 October 2005; received in revised form 2 February 2006; accepted 6 February 2006
Available online 15 March 2006

Abstract

Chagas' disease, caused by the *Trypanosoma cruzi* parasite, is one of the largest public health problems in the Western hemisphere, with 16–18 million people infected, and approximately 100 million people at risk. Many efforts towards the development of targeted antiparasitic agents have recently been described. Of interest, bisphosphonates, pyrophosphate analogs in which the oxygen bridge between the two phosphorus atoms has been replaced by a carbon substituted with different side chains, are able to inhibit the growth of *T. cruzi*. The enzyme *T. cruzi* farnesyl pyrophosphate synthase (TcFPPS) involved in the mevalonate pathway, has been recently identified as the target of bisphosphonates. The protein has 362 amino acids and a molecular mass of 41.2 kDa. Several sequence motifs found in other FPPSs are present in TcFPPS. In this study we have modeled the structure of TcFPPS based on the structure of the avian FPPS. We have characterized the interaction with its substrates, isopentyl pyrophosphate and dimethylallyl pyrophosphate, and the mechanism of inhibition by the potent bisphosphonate risedronate (K_i of 0.032 ± 0.002 μM) by means of molecular dynamics techniques. We propose that homorisedronate, which has an extra methylene and a K_i of 8.17 ± 1.36 μM, does not form strong hydrogen bonds with TYR 211 and THR 208, which may be responsible for its lower activity as compared to risedronate. Moreover, we were able to reproduce the structural changes that occur upon the binding of the third Mg^{2+} to the active site of the protein. Taken together, our results provide a structural model for the design of novel inhibitors that may prove useful for the treatment of Chagas' disease.

Keywords: Chagas' disease; Homology modeling; Molecular dynamics; Bisphosphonates; Farnesyl pyrophosphate synthase

1. Introduction

Chagas' disease (CD) also called *American trypanosomiasis*, is an infection caused by the parasite *Trypanosoma cruzi*. Worldwide, it is estimated that 16–18 million people are infected with CD; of those infected, 50,000 will die each year [1]. CD is the most important parasitic disease in Latin America in terms of its impact on national economies and public health systems [2]. Parasites are transmitted to humans in three ways: (1) by bloodfeeding *Triatomina*e bugs, which live in cracks and crevices of poor-quality houses, usually in rural areas; (2) through transfusion with infected blood; (3) congenitally, from infected mother to fetus [3]. There has been considerable interest in developing novel chemotherapeutic approaches, based on unique aspects of the structure and metabolism of this parasite.

It has been reported that during the proliferative stages of the parasite large quantities of inorganic pyrophosphate are found in *T. cruzi* acidocalcisomes and that pyrophosphate can be even more abundant than ATP [4]. This led to the idea that parasite growth might be inhibited in the presence of a stable analog of diphosphate. Taking this into account, bisphosphonates, pyrophosphate analogs in which the oxygen bridge between the two phosphorus atoms has been replaced by a carbon substituted with different side chains, have been proven to inhibit the growth in vitro and in vivo of the parasite [4–10]. Bisphosphonates represent an important class of drugs currently used to treat osteoporosis, Paget's disease and hypercalcemia due to malignancy. The enzyme farnesyl pyrophosphate synthase (FPPS), involved in the mevalonate pathway, has been identified as the target of bisphosphonates in

* Corresponding autor at: Oral and Pharyngeal Cancer Branch, National Institute of Dental and Craniofacial Research, NIH, Bethesda, MD, United States. Tel.: +1 301 402 0823; fax: +1 301 402 7432.
E-mail address: adrian@qi.fcen.uba.ar (A.G. Turjanski).

1093-3263/$ – see front matter © 2006 Elsevier Inc. All rights reserved.
doi:10.1016/j.jmgm.2006.02.001

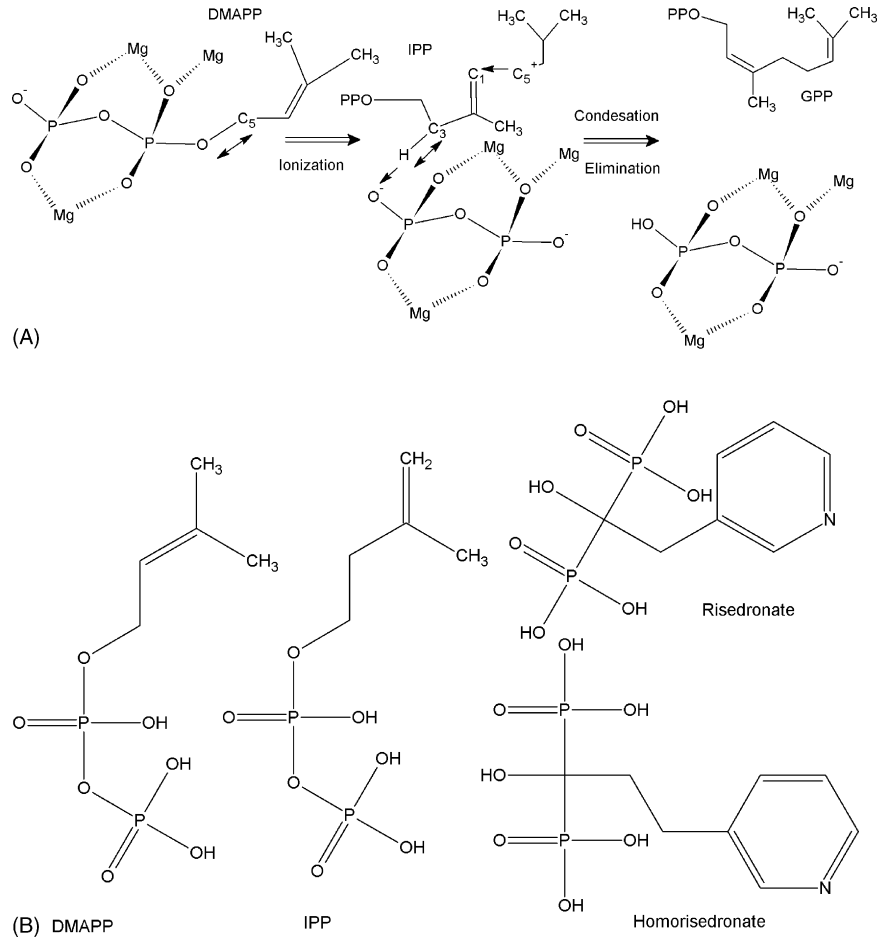

Scheme 1. (A) The proposed reaction mechanism for FPPS [9]. The substrate binds to the active site with 3 Mg^{2+} that labilize the C5–O bond of DMAPP generating an allylic carbocation that alkylates the C1 atom of IPP. In a second step, a DMAPP pyrophosphate oxygen serves as the catalytic base removing the IPP C3 pro-R hydrogen and thus allowing the double bond formation in the final product. (B) Chemical structure of DMAPP, IPP, RIS and HRIS.

different organisms [11–13]. This biosynthetic route leads to the formation of several products, among the most relevant ones are cholesterol and the nonsteroidal isoprenoids farnesyl pyrophosphate (FPP) and geranylgeranyl pyrophosphate (GGPP) of which the latter two can be used as substrates for post-translational protein prenylation. FPPS catalyzes the 1′-4 condensation of dimethylallyl pyrophosphate (DMAPP) with two molecules of isopentenyl pyrophosphate (IPP) to form first geranyl pyrophosphate (Scheme 1A) and in a subsequent step FPP [14]. The structure of apo- and ligand-bound avian FPPS have been solved [15,16] and recently the structures of unliganded *Staphylococcus aureus* FPPS (FPPS-Sa), as well as two *Escherichia coli* FPPS (FPPS-Ec) ternary complexes has been determined [9]. One of these ternary complexes contains IPP and the noncleavable DMAPP analogue dimethylallyl *S*-thiolodiphosphate (DMSPP) [17] and the other a bisphosphonate-bound structure containing IPP and the osteoporosis drug 1-hydroxy-2-(3-pyridinyl)ethylidene bisphosphonic acid, risedronate (RIS) [9]. RIS (Scheme 1B) is an aromatic nitrogen-containing bisphosphonate that inhibits *T. cruzi* FPPS (TcFPPS) with a K_i of 0.032 ± 0.002 μM [11]. Interestingly, the similar homorisedronate (HRIS) (Scheme 1B), which has an extra methylene, has a K_i of 8.17 ± 1.36 μM [11]. The active site of FPPS includes Mg^{2+} cations that are probably involved in ligand binding and catalysis. However, the different experimental structures exhibit 1, 2 or 3 Mg^{2+} ions [9,15,16], and the real role of these ions in the enzyme function is still an open question.

We report a thorough computational study of the structural characteristics of TcFPPS. We have developed a model of TcFPPS with its two substrates, IPP and DMAPP, docked in the active site based on the structure of the avian FPPS. We have evaluated the differences arising from binding 2 or 3 Mg^{2+} cations and propose a specific role for the third Mg^{2+} in the closing of the protein active site based on molecular dynamics simulations (MD). Moreover, we have modeled the interaction with risedronate and homorisedronate and provide structural information that may clarify the molecular basis of the difference in activity of these two similar compounds.

2. Methods

2.1. Sequence alignment

The amino acid sequence of TcFPPS was obtained from the protein database from NCBI (http://www.ncbi.nlm.nih.gov/protein) (gi:14647139). The PSI-BLAST [18] algorithm was used to identify homologous structures for TcFPPS by

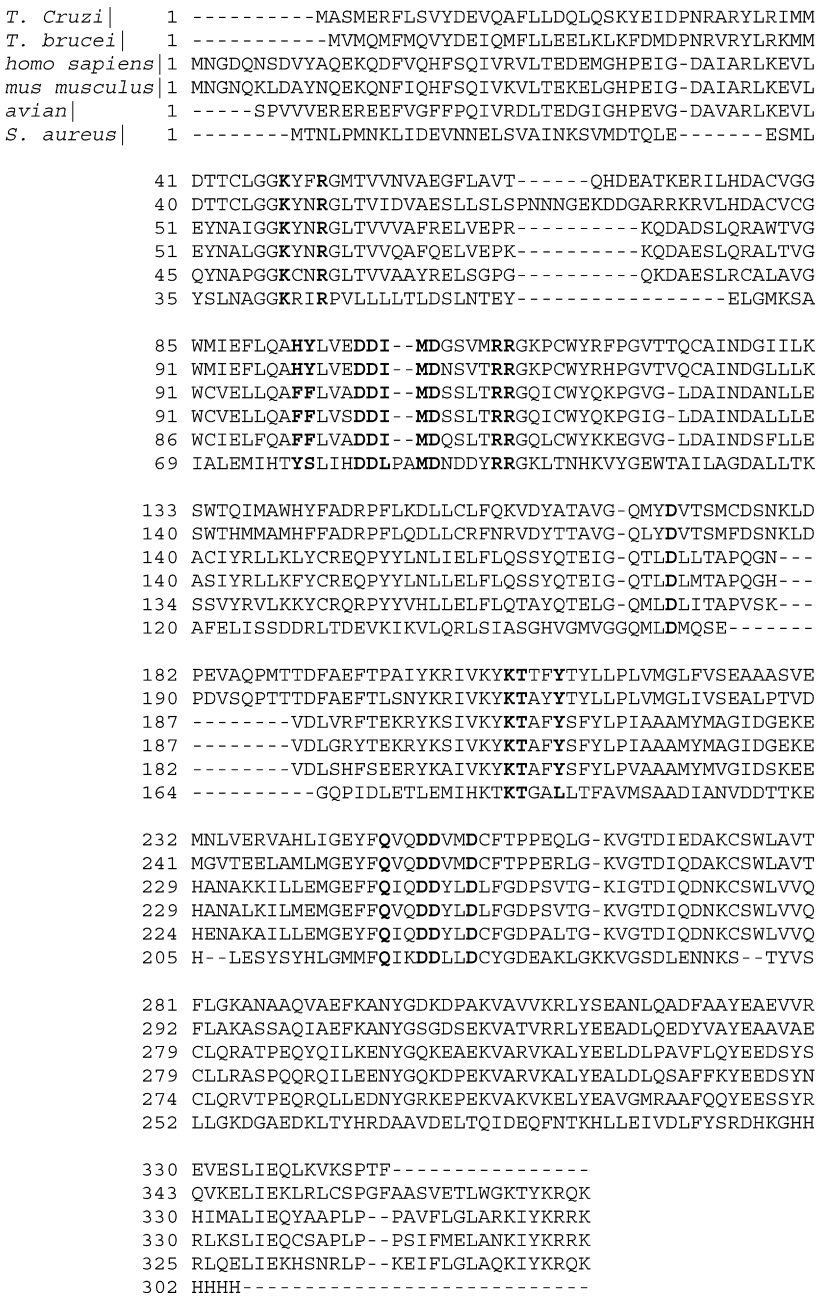

Fig. 1. The sequence alignment of FPPS from *T. cruzi*, *T. brucei*, human, *Mus musculus*, avian and *S. aureus* respectively produced by CLUSTALX. In bold style are highlighted the amino acids that have been shown to be part of the catalytic site.

searching the structural database of protein sequences in the Protein Data Bank (PDB) [19]. The FPPS crystal structures of avian (PDB codes 1FPS) (resolution 2.6 Å), 1UBV (resolution 2.5 Å) (without ligands and Mg^{2+}), 1UBW (with GPP and 2 Mg^{2+}) (resolution 2.5 Å), 1UBX (with FPP and 1 Mg^{2+}) (resolution 2.5 Å) and 1UBY (with DMAPP and 2 Mg^{2+}) (resolution 2.4 Å), the last four structures have two point mutations (P112A) and (P113S) [15,16], were selected as template structures for homology modeling of the TcFPPS enzyme. The selection of these structures was based on the highest sequence identity and similarity (36% identity and 50% similarity). Sequence alignments were created with ClustalX [20].

2.2. Homology modeling

The homology model was constructed using Swiss-PDBViewer version 3.7 [21–23]. As pointed above, the homology model of TcFPPS was based on the crystals structures of avian FPPS (1FPS, 1UBV, 1UBW, 1UBX and 1UBY) which share 36% identity and 50% similarity with the sequence of TcFPPS. Even though the sequences are nearly the same, we have used the four available structures to gain from conformational variances. While this project was being carried out the structure of human FPPS was deposited in the PDB (Kavanagh et al., to be published), PDB accession codes 1YV5, 1YQ7 and 1ZW5 (resolution 2.30, 2.20 and 2.00 Å,

respectively), thus we have also refined our model of TcFPPS using these structures as template, but no significant changes were observed. The quality of this model was examined by WHATCHECK [24]. As TcFPPS has an 11-mer region that is not found in the avian structure (amino acids SMCDSNKLDPE), a loop library derived from experimental structures was searched to find compatible loop fragments as implemented in Swiss-PDBViewer [25]. The selection of the loop structure was based on homology, energy and clash parameters [25]. Moreover, some of the reasonable loop structures, based on the above parameters, were discarded as they interfered with the formation of the protein dimer considering the avian X-ray structure. Based on the above assumptions we found a small subset of conformations that had small FF (force field) and PP (main force potential) values and selected one of them on the basis of the higher homology within the loop in the database and our loop. Interestingly, none of the loop conformations interacted with the active site. The entire three-dimensional models were subjected to molecular mechanics energy minimization calculations using the updated Cornell et al. force field, named parm99 within the AMBER 7.0 package distribution [26].

2.3. Complex preparation

The different protein complexes, TcFPPS with DMAPP, IPP and 2 Mg^{2+} (A1), TcFPPS with DMAPP and 2 Mg^{2+} (A2), TcFPPS with DMAPP and 3 Mg^{2+} (A3), TcFPPS with RIS and 2 Mg^{2+} (B1), TcFPPS with RIS and 3 Mg^{2+} (B2), TcFPPS with HRIS and 2 Mg^{2+} (C1) and TcFPPS with HRIS and 3 Mg^{2+} (C2) where assembled by RMS fit to the X-ray structures of avian, *S. aureus* and *E. coli* FPPS [9,15,16]. All complexes were subjected to molecular mechanics energy minimization calculations using the updated Cornell et al. force field [26].

2.4. Bisphosponates parameterization

Partial charges for the bisphosphonates were obtained using the restrained electrostatic fit (RESP) scheme [27]. Electrostatic potentials were computed using ab initio HF/6–31G** calculations using the Gaussian 98 package [28]. Most of the parameters for bisphosphonates were taken from the AMBER force field [26,29]. The parameters associated with the torsional degrees of freedom of the bisphosphonic acid were not available and were obtained by fitting them iteratively to reproduce the energy profiles obtained from HF/6–31G** calculations [29]. We protonated the bisphosphonates considering their pK_as and the magnesium binding, for RIS and HRIS, one oxygen not bound to magnesium was protonated.

2.5. Molecular dynamics

MD simulations were performed using the Amber force field [26], and the TIP3P model for water [30]. Parameters for the bisphosphonates are described above. In all cases, we used AMBER7 software package [31], the time step was 2 fs, the van der Waals interactions were smoothly cut-off at 10 Å. All

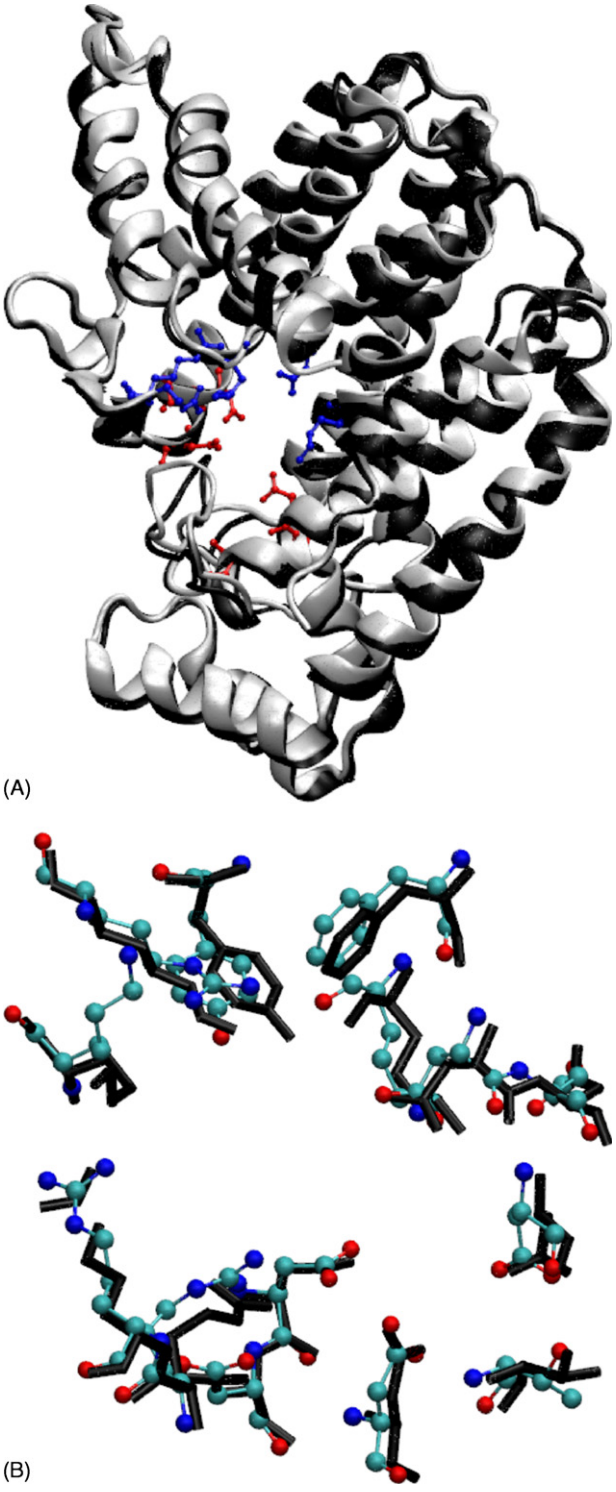

Fig. 2. (A) The model of TcFFPS in black cartoons aligned with the structure of avian FPPS (PDB: 1UBY) in white cartoons. In blue balls and sticks are depicted the basic amino acids present in the active site [ARG (51, 107, 108), LYS 48] and in red balls and sticks are depicted the acidic amino acids involved in the catalytic site, ASP (98, 99, 102, 170, 250, 251). (B) A zoom of the active site depicted in part (A) showing in black sticks the amino acids from our TcFPPS model and in balls and sticks the same amino acids for the avian FPPS. We have selected the amino acids depicted in (A) plus THR 208 and TYR 211.

hydrogen bonds were kept rigid by using the SHAKE algorithm [32]. The Berendsen thermostat [33] was used to maintain the desired temperature; all simulations were conducted at 300 K. In all cases, as mentioned above, the model structure was first refined by adding all hydrogen atoms and subsequent energy minimization with the SANDER module of AMBER 7. The protein was solvated in a cubic periodic box containing 17,330 water molecules. The particle mesh Ewald (PME) method [34] was used with a non-bonded cut-off of 10 Å. In each case for the residues outside a cap of 30 Å from the center of mass of the Mg^{2+} atoms an harmonic constraint of 4 kcal/mol/Å was applied. The residues included in the restraint are mostly loops that are away from the active site and have low sequence identity with the X-ray structures used to model the protein. As expected, under an unrestrained MD large oscillations in these regions occurred which produced distortions that altered the conformation of amino acids near the active site.

In each case the complex structures where first equilibrated for 80 ps keeping the whole protein fixed with a constraint of 4 kcal/mol/Å to allow the water and the ligands or inhibitors molecules to relax. A subsequent 100 ps of equilibration without restrains was carried out. After the equilibration phase we obtained 1 ns MD trajectory for every complex.

3. Results and discussion

The sequence alignment of FPPS from *T. cruzi* FPPS (gi|71425811|) with the sequences of the avian (gi|1065289|), *Homo sapiens* (gi|1346031|), *S. aureus* (gi|46015556|), *Mus musculus* (gi|15824695) and *T. brucei* (gi|71850184|) is shown in Fig. 1. As can be seen in the alignment, there is a significant sequence similarity among FPPSs from different organisms. We have highlighted the amino acids that have been shown to be part of the catalytic site. Two conserved Asp-rich motifs DDXXD (where X can be any amino acid), which are responsible for binding the Mg^{2+} atoms that make a salt bridge between the protein and the pyrophosphate moiety of DMAPP and the presence of conserved ARG and LYS amino acids that make salt bridges with the IPP pyrophosphate [9,15] can be found. As shown in Fig. 1, all these amino acids are also present in TcFPPS. One important feature of prenyltransferases is the regulation of the product chain length, two aromatic residues which are somehow conserved in FPPSs but are not present in higher chain length synthases have been proposed to be important for this process [35]. In TcFPPS the two Phe residues present in the human and avian are changed to HIS (93) and TYR (94). Interestingly, in *S. auereus* the second PHE residue is changed to SER.

Our model of TcFPPs is depicted in Fig. 2A. Even though the identity with the template structure is low (36%), as pointed above the critical amino acids for binding and catalysis are well conserved and it is expected that our model reflects the important characteristics of TcFPPS. The overall quality of the prediction, assessed by means of the WHATCHECK program [24], was good. There were no significance changes in the Ramachandran plot as compared to the avian structure as well as in the distribution of the φ/ψ angles of the model that are mostly within the allowed regions. TcFPPS has an 11-mer loop, not present in the human or avian FPPSs. This loop has been proposed to be near the active site and play an important role in enzyme activity [11]. Our results for the evaluation of different conformations of the loop, suggested that the accesible conformations do not seem to be involved in the catalytic site of the enzyme. For comparison, in Fig. 2B we have depicted the amino acids of the active site which are responsible for ligand binding in the avian FPPS, in our model, including ASP (98, 102, 170), ARG (51, 107, 108) and LYS 48. Indeed, the active pockets turn out to be very similar for these two enzymes.

We modeled the interaction of TcFPPS with IPP and DMAPP; the chemical structures are depicted in Scheme 1B, in which we docked the molecules as described in methods with 2 Mg^{2+}. The docked structure resembles those previously observed for the structure of other FPPSs [15,16]. However, some of the interactions where lacking because the amino acids side chains where rotated. In order to relax the structure we conducted molecular dynamics simulations for complex A1. Significant changes in the active site structure were observed upon relaxation, and most of the relevant reported interactions were formed. The 2 Mg^{2+} ions formed bonds to the DMAPP pyrophosphate moiety and salt bridges with ASP (98, 102, 170), as depicted in Fig. 3A. ARG (51, 107, 108) and LYS 48 formed salt bridges with the oxygen of the pyrophosphate moiety of IPP and DMAPP (Fig. 3A and B). THR 208 and GLN 247, postulated to be important in stabilizing the proposed

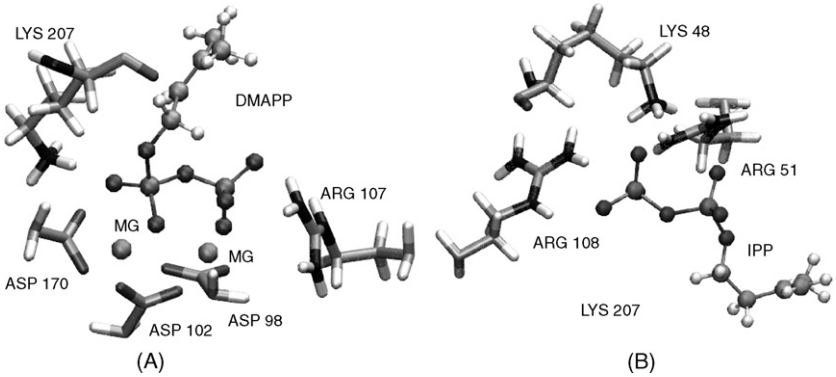

Fig. 3. (A) The active site of the model of TcFPPS with DMAPP. The amino acids that form salt bridges with Mg^{2+} and DMAPP are depicted in bonds rendering and DMAPP is in ball and stick. (B) IPP bound to TcFPPS in balls and sticks and basic amino acids surrounding pyrophosphate moiety are depicted in bonds rendering.

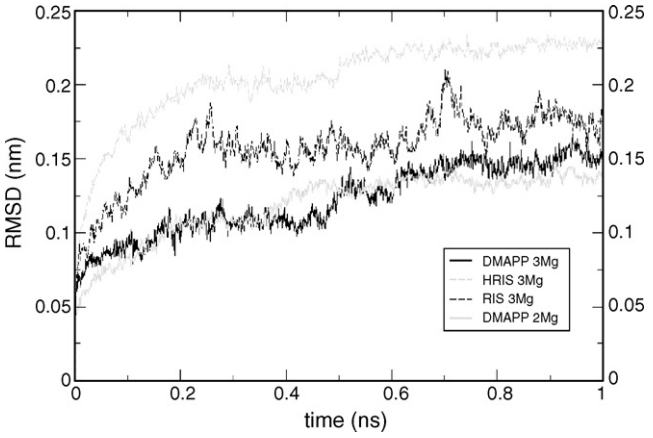

Fig. 4. The root mean square displacement (RMSD) of the backbone alpha carbon atoms of the protein with respect to the initial equilibrated configuration as a function of time, for the simulations of TcFPPS with DMAPP and 2 Mg^{2+}, with DMAPP and 3 Mg^{2+}, with RIS and 3 Mg^{2+} and with HRIS with 3 Mg^{2+}.

carbocation intermediate of the reaction [9] (Scheme 1A) are also located near DMAPP. In order to further relax the protein and examine the stability of the active site we performed a 1 ns MD simulation at 300 K. As seen in Fig. 4, the root mean square displacement (RMSD) of the backbone alpha carbon atoms of the protein with respect to the initial equilibrated configuration is around 0.14 nm. Moreover, no significant changes were observed in the active site conformation.

Although the structure of FPPS has been solved for different organisms the exact catalytic mechanism is not known. Mg^{2+} cations play an important role in the binding of DMAPP, possibly by stabilizing the pyrophosphate moiety and therefore labilizing the pyrophosphate–DMA aliphatic chain bond. In addition, Mg^{2+} cations are crucial for the binding of the bisphosphonates inhibitors. The structures of avian FPPS have 2 Mg^{2+} with DMAPP and geranyl pyrophosphate and 1 Mg^{2+} with FPP, on the other hand the structures of *S. aureus*, *E. coli* and human have 3 Mg^{2+} [9,15] (Kavanagh et al., to be published). The addition of a third Mg^{2+} seems to attract the more distant aspartates of the second DDXXD motif, thus closing the active site. To test this hypothesis we added the third magnesium to our ''open'' model of TcFPPS using the *E. coli* structure as template and conducted molecular dynamics simulations. After the equilibration phase, ASP (250, 251) moved towards the active site forming salt bridges with the third Mg^{2+}. The change in conformation of the acidic residues approaches the last part of the alpha helix expanding from residue 230 to 255 towards the active site. The new structure shown in Fig. 5A, is very similar to the structure of FPPS-Ec and human FPPS with 3 Mg^{2+}, and therefore shows again that our model is capturing the important features of TcFPPS. We performed up to 1 ns MD simulations and no further changes in the aspartates conformation were observed, and the protein remains stable, with a RMSD of 0.15 nm (Fig. 4). We have measured the distance from the nearest ASP 250 and ASP 251 oxygen to the central oxygen of the pyrophosphate moiety in DMA in the absence of the third Mg^{2+} (Fig. 5B). The mean distance was 0.56 ± 0.02 nm for ASP 250 and 0.8 ± 0.06 nm for ASP 251; when we added the third Mg^{2+}, the mean distances went to 0.4 ± 0.01 nm for ASP 250 and 0.46 ± 0.01 nm for ASP 251 (Fig. 5B). We have also performed the same simulations with 2 and 3 Mg^{2+} for the inhibitors RIS and HRIS (B1, B2, C1, C2), with similar results. As in the avian FPPS there was no binding pocket already formed for the third Mg^{2+}, based on our simulations, we propose that DMAPP or the

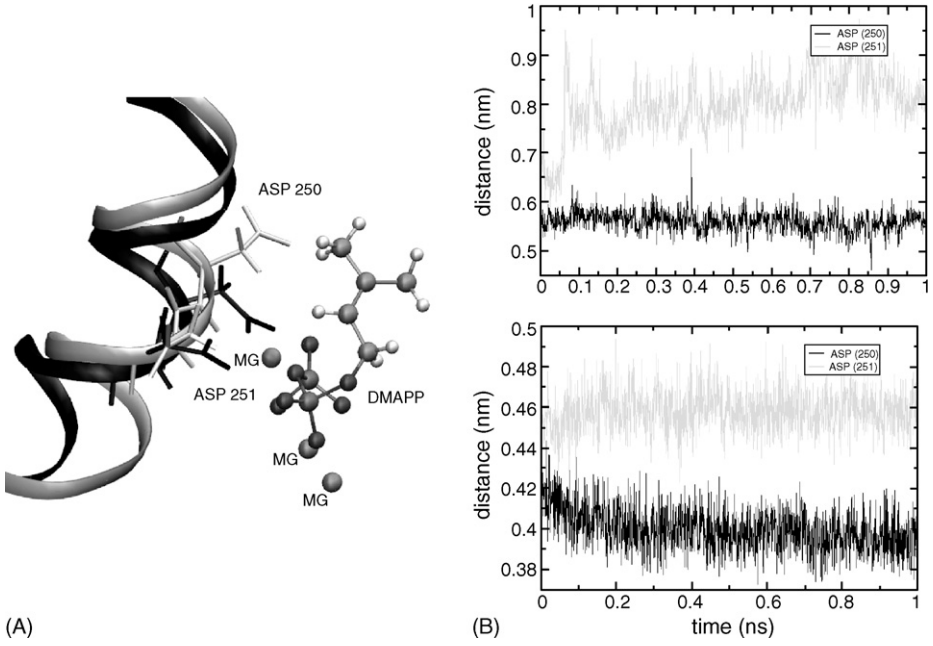

Fig. 5. Structural changes in TcFPPS upon binding of the third Mg^{2+}. (A) In cartoon rendering are depicted amino acids 247–256, in white the model with Mg^{2+} and in black the model with 3 Mg^{2+}. In ball rendering are shown ASP 250 and ASP 251 with turn towards Mg^{2+}. The DMAPP ligand is depicted in balls and sticks. This is a snapshot taken after 1 ns of MD simulation upon the addition of the third Mg^{2+} (B). The distances from the nearest ASP (250) and ASP (251) oxygen to the central oxygen of the pyrophosphate moiety in DMA in the absence (upper panel) and presence (lower panel) of the third Mg^{2+}.

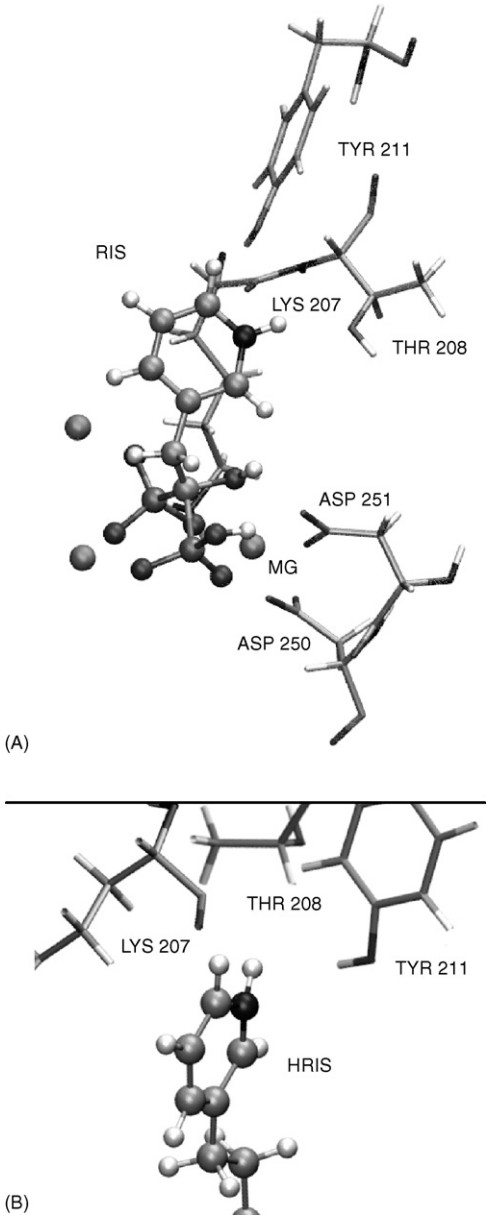

Fig. 6. (A) The structure of TcFPPS with RIS bound in the active site. RIS is depicted in balls and sticks and the relevant amino acids involved in direct interaction with the bisphosphonate are shown in bond rendering. (B) The aromatic ring of HRIS is shown in balls and sticks and LYS 207, THR 208 and TYR 211 in bond rendering.

bisphosphonates inhibitors bind to the enzyme that has 2 Mg^{2+}, and that then the third Mg^{2+} binds and closes the active site.

We have modeled the structure of TcFPPS bound to RIS and HRIS with 3 Mg^{2+} (B2, C2) in order to understand the inhibition mechanism of the drugs. RIS inhibits TcFPPS with a K_i of 0.032 ± 0.002 μM [11] and HRIS, which has an extra methylene, with a K_i of 8.17 ± 1.36 μM [11], what accounts for a difference in binding energy of around 3 kcal/mol. We have performed 1 ns MD simulations for both complexes. We observed that after an equilibration phase RIS binds to TcFPPS in a very similar manner as what has been observed for other FPPS [9] (Kavanagh et al., to be published). RIS formed salt bridges with the 3 Mg^{2+} cations, which in turn forms salt bridges with ASP (98, 102, 170, 250, 251). LYS 207 also contributes to the binding by forming a salt bridge with the bisphosphonic moiety of RIS. During the 1 ns simulation the protein structure remains stable, with a RMSD of 0.17 nm 2.4 Å (Fig. 4). Interestingly, the active site closed as pointed above when we added the 3 Mg^{2+} ions and ASP 250 formed hydrogen bonds with the protonated oxygen of the bisphosphonate and the hydroxyl group at C-1. These hydrogen bonds were formed 100% and 96% of the time in our 1 ns simulation, respectively (our criteria for measuring hydrogen bonds was a cut-off of 3.5 Å and 90°) (Fig. 6A). This may explain the higher activity observed for the bisphophosnates that have an hydroxyl group at the C-1 position [36]. The aromatic ring of RIS has a positive charged nitrogen that is able to form hydrogen bonds with the OH groups of THR 208 and TYR 211, and with the backbone carbonyl oxygen of LYS 207 (Fig. 6A). Using our previous cut-off, these three hydrogen bonds were formed 97%, 90% and 76% of the simulation time, respectively.

The structure of TcFPPS bound to HRIS is depicted in Fig. 6B. The RMSD of the 1 ns simulation is shown in Fig. 4. As expected, the binding mode of HRIS is quite similar to that of RIS, except for the aromatic ring. In our model the positive NH group of HRIS is only able to form an strong hydrogen bond with the carbonyl of LYS 207 (100% of the time), but not with THR 208 (32%) and TYR 211 (0%). This may explain the difference in activity observed between these two drugs, as the binding energy has a difference of only 3 kcal/mol, within the range of a hydrogen bond interaction. However, we cannot rule out the possibility that limitations of our model may lead to the differences observed.

We have performed a thorough computational study of the structural characteristics of TcFPPS. We proposed a model for the active site that may be useful for the future design of novel inhibitors for the treatment of Chagas' disease. Our model could reproduce the interactions with its substrates, the structural changes upon Mg^{2+} binding and the inhibition by two bisphosphonates. It has been proposed that nitrogen containing bisphoshponates are carbocation transition state analogs of the reaction catalyzed by FPPSs [37]. In this scenario our model supports this mechanism for their inhibition of TcFPPS. However, aliphatic bisphoshponates are also potent inhibitors of TcFPPS [36], and further experimental and theoretical studies should be conducted to clarify this point. Finally, taking into account that our model captures important structural characteristics observed in previously solved FPPSs structures, specifically the recently solved human FPPS, it is expected that most of the drugs, as has been shown for bisphosphonates, that inhibit the human FPPS may inhibit the TcFPPS.

Acknowledgments

We thank Dr. Estrin for his help and advice and Dr. Silvio Gutkind for his comments and patience. A.G.T. acknowledge financial support from Fundación Antorchas and Universidad de Buenos Aires, L. Sigman and V. Sanchez are fellows from the Universidad de Buenos Aires.

References

[1] J.A. Urbina, R. Docampo, Specific chemotherapy of Chagas' disease: controversies and advances, Trends Parasitol. 19 (2003) 495–501.

[2] M.A. Miles, M.D. Feliciangeli, A.R. de Arias, American trypanosomiasis (Chagas' disease) and the role of molecular epidemiology in guiding control strategies, BMJ 326 (2003) 1444–1448.

[3] L.V. Kirchhoff, American trypanosomiasis (Chagas' disease)—a tropical disease now in the United States, N. Engl. J. Med. 329 (1993) 639–644.

[4] J.A. Urbina, B. Moreno, S. Vierkotter, E. Oldfield, G. Payares, C. Sanoja, B.N. Bailey, W. Yan, D.A. Scott, S.N. Moreno, R. Docampo, *Trypanosoma cruzi* contains major pyrophosphate stores, and its growth in vitro and in vivo is blocked by pyrophosphate analogs, J. Biol. Chem. 274 (1999) 33609–33615.

[5] J.E. Dunford, K. Thompson, F.P. Coxon, S.P. Luckman, F.M. Hahn, C.D. Poulter, F.H. Ebetino, M.J. Rogers, Structure–activity relationships for inhibition of farnesyl diphosphate synthase in vitro and inhibition of bone resorption in vivo by nitrogen-containing bisphosphonates, J. Pharmacol. Exp. Ther. 296 (2001) 235–242.

[6] J.M. Sanders, Y. Song, J.M. Chan, Y. Zhang, S. Jennings, T. Kosztowski, S. Odeh, R. Flessner, C. Schwerdtfeger, E. Kotsikorou, G.A. Meints, A.O. Gomez, D. Gonzalez-Pacanowska, A.M. Raker, H. Wang, E.R. van Beek, S.E. Papapoulos, C.T. Morita, E. Oldfield, Pyridinium-1-yl bisphosphonates are potent inhibitors of farnesyl diphosphate synthase and bone resorption, J. Med. Chem. 48 (2005) 2957–2963.

[7] Y. Ling, G. Sahota, S. Odeh, J.M. Chan, F.G. Araujo, S.N. Moreno, E. Oldfield, Bisphosphonate inhibitors of *Toxoplasma gondi* growth: in vitro, QSAR, and in vivo investigations, J. Med. Chem. 48 (2005) 3130–3140.

[8] F. Cheng, E. Oldfield, Inhibition of isoprene biosynthesis pathway enzymes by phosphonates, bisphosphonates, and diphosphates, J. Med. Chem. 47 (2004) 5149–5158.

[9] D.J. Hosfield, Y. Zhang, D.R. Dougan, A. Broun, L.W. Tari, R.V. Swanson, J. Finn, Structural basis for bisphosphonate-mediated inhibition of isoprenoid biosynthesis, J. Biol. Chem. 279 (2004) 8526–8529.

[10] S.H. Szajnman, E.L. Ravaschino, R. Docampo, J.B. Rodriguez, Synthesis and biological evaluation of 1-amino-1,1-bisphosphonates derived from fatty acids against *Trypanosoma cruzi* targeting farnesyl pyrophosphate synthase, Bioorg. Med. Chem. Lett. 15 (2005) 4685–4690.

[11] A. Montalvetti, B.N. Bailey, M.B. Martin, G.W. Severin, E. Oldfield, R. Docampo, Bisphosphonates are potent inhibitors of *Trypanosoma cruzi* farnesyl pyrophosphate synthase, J. Biol. Chem. 276 (2001) 33930–33937.

[12] B.E. van, E. Pieterman, L. Cohen, C. Lowik, S. Papapoulos, Farnesyl pyrophosphate synthase is the molecular target of nitrogen-containing bisphosphonates, Biochem. Biophys. Res. Commun. 264 (1999) 108–111.

[13] B.E. van, E. Pieterman, L. Cohen, C. Lowik, S. Papapoulos, Nitrogen-containing bisphosphonates inhibit isopentenyl pyrophosphate isomerase/farnesyl pyrophosphate synthase activity with relative potencies corresponding to their antiresorptive potencies in vitro and in vivo, Biochem. Biophys. Res. Commun. 255 (1999) 491–494.

[14] M.N. Ashby, P.A. Edwards, Identification and regulation of a rat liver cDNA encoding farnesyl pyrophosphate synthetase, J. Biol. Chem. 264 (1989) 635–640.

[15] L.C. Tarshis, M. Yan, C.D. Poulter, J.C. Sacchettini, Crystal structure of recombinant farnesyl diphosphate synthase at 2.6-A resolution, Biochemistry 33 (1994) 10871–10877.

[16] L.C. Tarshis, P.J. Proteau, B.A. Kellogg, J.C. Sacchettini, C.D. Poulter, Regulation of product chain length by isoprenyl diphosphate synthases, Proc. Natl. Acad. Sci. U.S.A. 93 (1996) 15018–15023.

[17] R.M. Phan, C.D. Poulter, Synthesis of (*S*)-isoprenoid thiodiphosphates as substrates and inhibitors, J. Org. Chem. 66 (2001) 6705–6710.

[18] S.F. Altschul, T.L. Madden, A.A. Schaffer, J. Zhang, Z. Zhang, W. Miller, D.J. Lipman, Gapped BLAST and PSI-BLAST: a new generation of protein database search programs, Nucl. Acids Res. 25 (1997) 3389–3402.

[19] H.M. Berman, T. Battistuz, T.N. Bhat, W.F. Bluhm, P.E. Bourne, K. Burkhardt, Z. Feng, G.L. Gilliland, L. Iype, S. Jain, P. Fagan, J. Marvin, D. Padilla, V. Ravichandran, B. Schneider, N. Thanki, H. Weissig, J.D. Westbrook, C. Zardecki, The protein data bank, Acta Crystallogr. D. Biol. Crystallogr. 58 (2002) 899–907.

[20] F. Jeanmougin, J.D. Thompson, M. Gouy, D.G. Higgins, T.J. Gibson, Multiple sequence alignment with Clustal X, Trends Biochem. Sci. 23 (1998) 403–405.

[21] M.C. Peitsch, ProMod and Swiss-model: internet-based tools for automated comparative protein modelling, Biochem. Soc. Trans. 24 (1996) 274–279.

[22] T. Schwede, J. Kopp, N. Guex, M.C. Peitsch, SWISS-MODEL: an automated protein homology-modeling server, Nucl. Acids Res. 31 (2003) 3381–3385.

[23] N. Guex, M.C. Peitsch, SWISS-MODEL and the Swiss-PdbViewer: an environment for comparative protein modeling, Electrophoresis 18 (1997) 2714–2723.

[24] R.W. Hooft, G. Vriend, C. Sander, E.E. Abola, Errors in protein structures, Nature 381 (1996) 272.

[25] M.J. Sippl, Calculation of conformational ensembles from potentials of mean force. An approach to the knowledge-based prediction of local structures in globular proteins, J. Mol. Biol. 213 (1990) 859–883.

[26] J.M. Wang, P. Cieplak, P.A. Kollman, How well does a restrained electrostatic potential (RESP) model perform in calculating conformational energies of organic and biological molecules? J. Comput. Chem. 21 (2000) 1049–1074.

[27] C.M. Breneman, K.B. Wiberg, Determining atom-centered monopoles from molecular electrostatic potentials—the need for high sampling density in formamide conformational-analysis, J. Comput. Chem. 11 (1990) 361–373.

[28] Gaussian 98, Rev. A7, Gaussian, Inc., Pittsburgh, PA, 1998.

[29] W.D. Cornell, P. Cieplak, C.I. Bayly, I.R. Gould, K.M. Merz, D.M. Ferguson, D.C. Spellmeyer, T. Fox, J.W. Caldwell, P.A. Kollman, A 2nd generation force-field for the simulation of proteins, nucleic-acids, and organic-molecules, J. Am. Chem. Soc. 117 (1995) 5179–5197.

[30] W.L. Jorgensen, J. Chandrasekhar, J.D. Madura, R.W. Impey, M.L. Klein, Comparison of simple potential functions for simulating liquid water, J. Chem. Phys. 79 (1983) 926–935.

[31] Amber 7, University of California, San Francisco, 2002.

[32] J.P. Ryckaert, G. Ciccotti, H.J.C. Berendsen, Numerical-integration of cartesian equations of motion of a system with constraints—molecular-dynamics of *N*-alkanes, J. Comput. Phys. 23 (1977) 327–341.

[33] H.J.C. Berendsen, J.P.M. Postma, W.F. Vangunsteren, A. Dinola, J.R. Haak, Molecular-dynamics with coupling to an external bath, J. Chem. Phys. 81 (1984) 3684–3690.

[34] U. Essmann, L. Perera, M.L. Berkowitz, T. Darden, H. Lee, L.G. Pedersen, A smooth particle mesh Ewald method, J. Chem. Phys. 103 (1995) 8577–8593.

[35] L.C. Tarshis, P.J. Proteau, B.A. Kellogg, J.C. Sacchettini, C.D. Poulter, Regulation of product chain length by isoprenyl diphosphate synthases, Proc. Natl. Acad. Sci. U.S.A. 93 (1996) 15018–15023.

[36] S.H. Szajnman, A. Montalvetti, Y. Wang, R. Docampo, J.B. Rodriguez, Bisphosphonates derived from fatty acids are potent inhibitors of *Trypanosoma cruzi* farnesyl pyrophosphate synthase, Bioorg. Med. Chem. Lett. 13 (2003) 3231–3235.

[37] M.B. Martin, W. Arnold, H.T. Heath III, J.A. Urbina, E. Oldfield, Nitrogen-containing bisphosphonates as carbocation transition state analogs for isoprenoid biosynthesis, Biochem. Biophys. Res. Commun. 263 (1999) 754–758.